NJC

ROYAL SOCIETY OF CHEMISTRY

PAPER

View Article Online
View Journal | View Issue

Cite this: *New J. Chem.*, 2023, **47**, 7312

In situ/photoinduced fabrication of Zn/ZnO nanoscale hetero-interfaces with concomitant generation of solar hydrogen†

Priti A. Mangrulkar,*[ab] Nilesh R. Manwar,[ac] Anushree A. Chilkalwar,[a] Aparna S. Deshpande[a] and Sadhana S. Rayalu*[a]

In the present investigation, we report the formation of a metal–metal oxide (Zn/ZnO) nanoscale heterointerfac with concomitant hydrogen generation. The synthesis process is simple and involves the optical illumination of Zn nanoparticles (Zn(NP)) suspended in water. The concomitant hydrogen (H_2) evolution during synthesis was found to be linear, and it is dependent on the growth of the Zn/ZnO nano interface. The progressively increasing amount of ZnO relative to Zn(NP) was a limiting factor in H_2 evolution. Two different Zn/ZnO nanoscale heterointerfaces were created and samples were extracted at two different stages of the illumination process. The first sample, extracted from the most reactive illumination phase and named Zn(NP)/ZnO-R, had the highest hydrogen evolution reaction (HER) rate. The second sample, extracted from a less reactive illumination phase and named Zn(NP)/ZnO-S, had a lower HER rate. These *in situ* (solar light-induced) samples were characterized by XRD, HRTEM, and other methods. The optoelectronic features and the photoelectrochemical (PEC) investigations showed the optimal light-harvesting ability of Zn(NP)/ZnO-R and the effective separation of photoexcited charge carriers, leading to remarkable HER performance. During the visible-light-induced (*in situ*) conversion of Zn(NP) to Zn(NP)/ZnO-R, a concurrent HER rate of 1115 μmol h^{-1} was observed. Indeed, the photocurrent density value of the Zn(NP)/ZnO-R catalyst is significantly higher than that of Zn(NP)/ZnO-S, pristine Zn(NP), and ZnO. Thus, this study provides new insights into the optimal fabrication of the Zn(NP)/ZnO interface for PEC application with concomitant solar hydrogen generation.

Received 4th November 2022,
Accepted 19th February 2023

DOI: 10.1039/d2nj05431k

rsc.li/njc

Introduction

Efficient energy harvesting and storage through sustainable methods is crucial to meet the growing global energy needs. The conversion of photons from solar energy into chemicals appears to be a highly promising approach in this regard. To achieve high photon conversion efficiency, it is necessary to identify and study low-cost, stable, and highly efficient photocatalysts.

Recently, metal/semiconductor nanostructures have drawn attention from researchers due to their unique properties, such as quantum confinement and surface plasmonic effects, which are not present in their bulk counterparts. The development of metal/oxide nanoscale interfaces is significant for their wide range of optoelectronic applications.[1] Both top-down and bottom-up approaches have been employed for the synthesis of nanomaterials. The mechano-synthetic approach is considered a green technique due to it being a zero-waste process and due to the absence of harmful chemicals.[2] Both top-down and bottom-up approaches have been employed for the synthesis of nanomaterials. The metal–oxide (MO) nanosystem interfaces have gained attention for their unique optoelectronic features and multifunctional characteristics.[3] To improve the photon conversion efficiency, researchers can employ one of the following methods: (1) inclusion of plasmonic metals or photosensitizers, (2) surface modification through defects or doping, or (3) combining with other metal or metal-free catalysts. Zn/ZnO nanostructures are unique among the metal–oxide systems that have been explored due to the formation of the heterojunction at the interface of the composite material. Zinc and Zn-based materials are abundant on the earth and possess excellent electronic properties, including a high n-type carrier concentration and carrier mobility of ~130 cm^2 V^{-1} s^{-1} at room temperature.[4] However, ZnO's large bandgap limits its practical

[a] *Environmental Materials Division, CSIR-National Environmental Engineering Research Institute, Nehru Marg, Nagpur, 440 020, MH, India. E-mail: priti1804@gmail.com, s_rayalu@neeri.res.in*
[b] *Shri Ramdeobaba College of Engineering and Management, Katol Road, Nagpur, 440 013, MH, India*
[c] *Institute of Physical Chemistry, Polish Academy of Sciences, Kasprzaka 44/52, 01-224, Warsaw, Poland*

† Electronic supplementary information (ESI) available: Supporting figures. See DOI: https://doi.org/10.1039/d2nj05431k

application as a visible-light-active photocatalyst, which is why research efforts are focused on expanding its spectral response by using any one of the methods mentioned earlier. Currently, researchers are interested in analyzing the efficacy of metal–metal oxide semiconductors.[5,6]

Many research articles have focused on synthesizing core–shell metal–metal oxide nanostructures and heterojunctions.[7,8] The close proximity of the metal core (*e.g.* Zn) and the corresponding metal oxide (ZnO) creates strong synergy, which enhances charge separation and transfer. The synthesis of Zn–ZnO nanoparticles has been achieved through laser ablation using zinc and sodium dodecyl sulfate (SDS) as the starting materials.[7] The size of the nanoparticles can be adjusted by varying the concentration of SDS. Hydrothermal routes have been used to synthesize self-assembled ZnO nanorods into 3D spherical shells on Zn sphere cores, which have potential applications in nanoelectronics, nanophotonics, and nanomedicine.[8] Zn–ZnO core–shell structures have also been formed through solid–vapor deposition,[9] thermal evaporation,[10,11] electrodeposition,[12] ultrasonic irradiation,[13] hot filament chemical vapor deposition, and other methods.[12] The applications of these synthesized Zn–ZnO core–shell structures are varied, with some being used for photoemission, sensing, and photoelectronic characteristics.[5,11,14,15]

The synthesis of Zn–ZnO composites without well-defined core–shell structures has also been explored for their characteristic applications.[5,10–12,15] However, many of these routes involve energy-intensive steps, stringent experimental conditions, and the use of expensive chemicals. The thermochemical splitting of the Zn/ZnO cycle for solar hydrogen production may require temperatures as high as 1000–1200 K.[16]

In this investigation, Zn/ZnO heterostructures were successfully synthesized through a simple illumination method using Zn nanoparticles as the precursor. Zn nanoparticles have been reported to exhibit plasmonic peaks in both the UV (4.8 eV) and IR (1.2 eV)[17,18] regions, and they have the unique ability to manipulate light over a broad spectrum through plasmonic decay processes.[13,18,19] Upon illumination with a UV-Visible source, strong absorption occurs due to the surface plasmon resonance (SPR) effect. The Zn nanoparticles are converted into ZnO through hydrolysis in water and subsequent condensation, resulting in hydrogen generation. Two different types of Zn/ZnO heterostructures can be formed depending on the extent of illumination, with varying Zn : ZnO ratios. The first type, Zn(NP)/ZnO-R (reactive), generated high hydrogen evolution reaction (HER) rates, while the second type, Zn(NP)/ZnO-S (spent), generated lower HER rates. The formation of the Zn/ZnO interface was accompanied by H_2 evolution. The samples were characterized and tested for their photoelectrochemical (PEC) performance. The significant increase in photocurrent density and high HER (1115 μmol h^{-1}) for Zn(NP)/ZnO-R led to the optimized, *in situ* fabrication of the Zn(NP)/ZnO interface.

Results and discussion

Fig. 1 exhibits powder X-ray diffraction (XRD) patterns of Zn(NP), Zn(NP)/ZnO(R), and Zn(NP)/ZnO(S) samples. The XRD

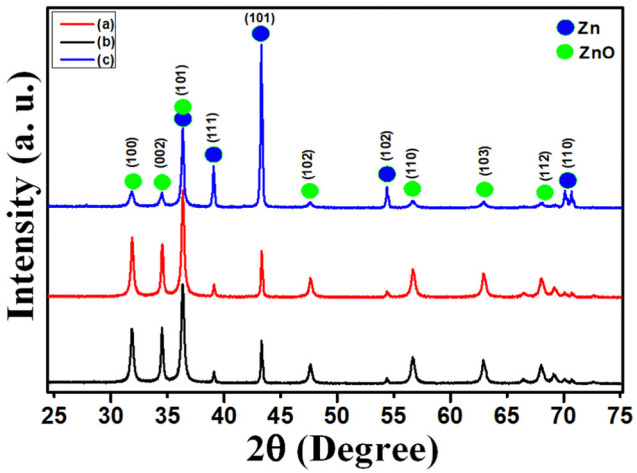

Fig. 1 XRD overlay showing the varying Zn:ZnO ratio (a) Zn(NP)/ZnO(R), (b) Zn(NP)/ZnO(S), and (c) Zn(NP).

pattern of ZnO shows prominent reflections at 2θ values of 31.7°, 34.4°, and 36.2°, arising from (101), (004), and (200) respective lattice planes corresponding to wurtzite structures of ZnO [JCPDS 36-1451].[20,21] The reflections from Zn metal at 43.4°, 54.5°, and 70.7° arising from (101), (003), and (200) lattice planes are seen distinctly. The co-existence of Zn and ZnO is very well evident from the XRD data. As such, zinc nanopowder (Zn(NP)) shows the predominant presence of the Zn metallic phase in the sample. The significant broadening observed in these XRD bands is a characteristic feature of nano-sized crystalline domains. A profound shift in the XRD spectra of Zn(NP)/ZnO-S is a noticeable feature in the broad XRD spectrum. However, the XRD comparison shows that the ratio of Zn : ZnO reduces as we go from the reactive to the spent condition.

High-resolution transmission electron microscopy (HRTEM) images provide further insight into the morphology of primary constituent particles in different samples. In Fig. 2(a), highly oriented nanocrystallites are a prominent feature of Zn(NP)/ZnO(R). Distinct grain boundaries with defined grain morphologies can be very well observed. However, distorted grain structures are well evident in the case of Zn(NP)/ZnO(S) (Fig. 2(b)). The lattice planes corresponding to ZnO and Zn are well indexed. The random orientation of fringes is indicative of the polycrystalline nature and also the heterogeneity of exposed lattice planes. The selected area electron diffraction (SAED) picture is in tune with the HRTEM results. The bright ring in the case of the Zn/ZnO composite with the innermost broad ring corresponding to the interplanar distance (d) 2.8 nm and the outer corresponding to d value 2.4, 2.08, and 1.47 nm of ZnO and Zn, respectively, are well noted. However, the SAED patterns of Zn(NP)/ZnO(S) showed variation in terms of brightness.

The large width and rather poor intensity of the obscured diffraction rings seen in Fig. 2(a) are well-reported features of nanosized composite samples having a low crystalline nature and with a strained lattice structure, arising due to certain microstructural defects. Zn/ZnO interface formation in the case of Zn(NP)/ZnO(R) is visible from the HRTEM. These interfaces

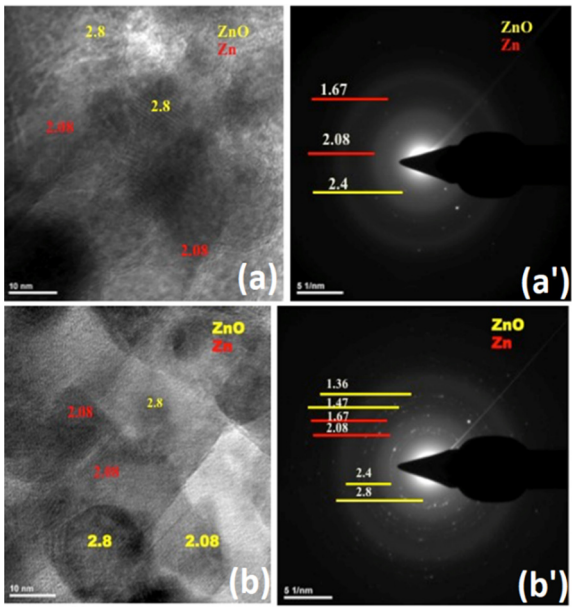

Fig. 2 HRTEM and SAED pattern for (a) Zn(NP)/ZnO(R) and (b) Zn(NP)/ZnO(S).

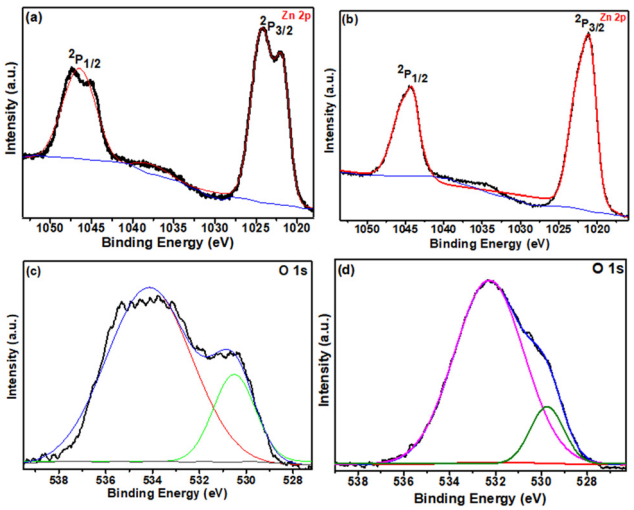

Fig. 3 Core level XPS spectra of Zn 2p for (a) Zn(NP)/ZnO(R) and (b) Zn(NP)/ZnO(S), and core level XPS spectra of O 1s for (c) Zn(NP)/ZnO(R) and (d) Zn(NP)/ZnO(S).

may play a vital role in the better activity of the composite metal–semiconductor nanostructures. HRTEM data shown in Fig. 2 bring out the presence of both ZnO and Zn contributions in the two samples. The energy-dispersive X-ray (EDX) analysis pattern shows a higher atomic % of Zn in the case of Zn(NP)/ZnO(R) than Zn(NP)/ZnO(S) [see ESI,† Fig. S1(a and b)]. The creation of oxygen vacancies and Zn interstitials could represent this state of disorder, and thus the observation appears to be consistent with the emergent picture stated above.

X-Ray photoelectron spectroscopy (XPS) data for Zn(NP)/ZnO(R) and Zn(NP)/ZnO(S) are represented in Fig. 3. Showing the core level XPS spectra of Zn 2p and O 1s contributions. In Zn(NP)/ZnO(R), the Zn $2P_{3/2}$ is located at 1021 eV with a tailing on the higher eV side. This mainly corresponds to ZnO, possibly with a tiny contribution of Zn metal. On the other hand, the Zn $2P_{3/2}$ for the Zn(NP)/ZnO(S) sample shows two prominent peaks, which correspond to Zn(II) as well as Zn (0) [Fig. 3(a and b)]. The possibility of hydroxide-type phases for this sample cannot be ruled out. Based on the XRD and EDX analysis stated above, it seems that free Zn metal in the sample decreases in quantity as we go from reactive (Zn(NP)/ZnO-R) to the spent (Zn(NP)/ZnO-S) catalyst system. The emergence of the Zn $2P_{3/2}$ contribution at the higher binding energy of 1024.1 eV represents Zn (0) interstitials created in the surface layer of ZnO due to enhanced oxygen vacancy formation.[22] The values of the split spin–orbit components (Δ) for zinc metal match well with the reference of 23 eV.

The higher content of oxygen vacancies in Zn(NP)/ZnO(S) as compared to Zn(NP)/ZnO(R) is also reflected in the O 1s data [Fig. 3(c and d)]. More specifically, the enhanced contribution towards higher binding energy in the O 1s data for Zn(NP)/ZnO(S) suggests the presence of a high concentration of oxygen vacancies, which pushes the energies of neighboring oxygen atoms in such a way as to lead to higher binding energy shift in the O 1s XPS.

Raman spectra for the Zn(NP)/ZnO-R and Zn(NP)/ZnO-S samples were analyzed (see ESI,† Fig. S2). The presence of metallic Zn or otherwise can be indirectly inferred from the nature of the background rising towards lower wavenumbers. It may be seen that in going from reactive to spent conditions, the metallic-like Raman background signature is reduced, which is consistent with the other data discussed above.

Factors influencing the formation of Zn/ZnO nanoscale heterojunctions

Photoinduced Zn/ZnO heterostructures were synthesized by employing a simple route of illuminating Zn(NP) in water by a suitable light source as detailed in the experimental section. The tungsten filament lamp was chosen as a source of illumination based on its spectral characteristics (Fig. S3, ESI†) as it comprises UV-Vis-NIR radiations. The formation of the Zn/ZnO heterointerface is governed by two factors; incident photons and temperature. The influence of both these factors can be indirectly studied and interpreted as a function of the hydrogen generated during the synthesis.

The synthesis of Zn/ZnO was carried out precisely in the same way as mentioned earlier in the presence and absence of an illumination source. The amount of hydrogen evolved was observed in both cases (with and without illumination). Fig. 4 shows the impact that the incident photons have on the photocatalytic activity during the formation of the Zn/ZnO heterostructure.

The rate of hydrogen evolution was remarkably higher in the presence of light (1115 μmol h^{-1}) than in its absence (26 μmol h^{-1}). This 40-fold increase in the rate clearly highlights the importance of *in situ* (photoinduced) formation of the catalyst (Zn(NP)/ZnO(R)). In the absence of light, zinc, which is the starting material, remains inactive, as its plasmonic effects

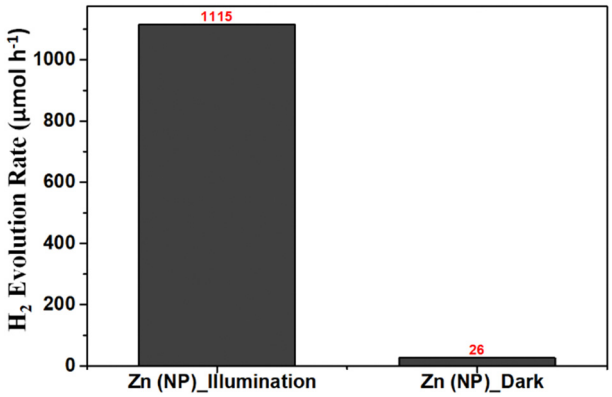

Fig. 4 Effect of the presence of light on the formation of the Zn/ZnO heterostructure.

do not come into play in the charge transfer process. However, in the presence of light, zinc nanoparticles absorb the incident photons, and the surface plasmon resonance (SPR) effect leads to several important reactions, which include the field-focusing effect of zinc nanoparticles on ZnO particles, light scattering and *in situ* heating.

The tungsten filament lamp used as a source of illumination mostly comprises Vis-NIR light and a small fraction of UV. The NIR component of light in addition to the plasmonic heat generated by Zn(NP) can raise the temperature of the solution. Thus, the temperature can also have a significant part to play in the formation of the Zn/ZnO interface. It was attempted to synthesize the Zn/ZnO heterostructures by providing photons using a Solar AM 1.5 and UV-Visible light source of illumination (NIR component is low). The concomitant HER was observed to 8.6 and 19.5 μmol h^{-1}, respectively, which is quite low thus illustrating the dual role of temperature and photons in the synthesis of highly efficient Zn/ZnO heterostructures.

To understand the exact role of the Zn/ZnO heterointerface system, it was considered worthwhile to perform a series of experiments on heat treating the samples in air. The Zn nanopowder was heated for 1 and 4 hours, respectively (denoted as Zn/ZnO-1 and Zn/ZnO-4) in the air, and its photocatalytic performance was checked. Table 1 indicates the values obtained for the rate of hydrogen evolution in the dark and under illumination. The obtained data clearly indicate that the HER goes down in samples subjected to prolonged heating. This can be attributed to the excess surface oxidation of metallic Zn to ZnO, wherein the benefit of plasmonic heat is reduced significantly due to the thick layer of ZnO, which hampers the effective charge transfer mechanism of the Zn/ZnO interface and degrades the field focusing effect.

Table 1 Effect of heat treatment on the catalytic activity of the Zn/ZnO interface

	H_2 evolution rate (μmol h^{-1})	
Photocatalyst	Dark	Illumination
Zn/ZnO-1	6.9	584
Zn/ZnO-4	6.0	578

Photoelectrochemical measurements

The photoelectrochemical (PEC) performance of the as-purchased (Zn(NP) & ZnO) and Zn/ZnO heterostructure samples (Zn(NP)/ZnO(R) & Zn(NP)/ZnO(S)) were examined through simple linear scan voltammetry, *i.e.* current density *vs.* potential (*I–V*) characteristic plot. The *I–V* plots are depicted in Fig. 5 with a low current density as measured for bare ZnO under dark conditions. Comparatively, all these photoanodes have achieved high current density under one sun conditions (Solar AM 1.5). Table 2 shows the detailed comparison of the obtained current density values at zero potential.

At zero bias, the maximum current density of 3.85 mA cm^{-2} was observed in the case of Zn(NP)/ZnO-R, which was nearly three times higher than that of Zn(NP)/ZnO-S. This remarkable enhancement in the current density is ascribed due to the optimal Zn/ZnO heterointerface of Zn(NP)/ZnO-R. Thus, the current density for Zn/ZnO heterostructures is significantly higher than the reported values for Zn/ZnO and ZnO alone.[12] The photocurrent density for ZnO, Zn(NP), Zn(NP)/ZnO-S, and Zn(NP)/ZnO-R is summarized in Table 2. The efficiency has been normalized with respect to the area of exposure and the amount of material that was being used.

It is evident that while all the samples show a notable photoresponse, the superior photocurrent characteristics are exhibited by the Zn(NP)/ZnO-R sample. Thus, it signifies the formation of a highly efficient Zn/ZnO heterointerface. This optimal interface plays an important role in such high photocatalytic activity.

Photoinduced formation of the Zn(NP)/ZnO heterointerface and plausible reaction mechanism

The effective interface between Zn(NP) and ZnO is obtained by a simple illumination route, which is schematically represented

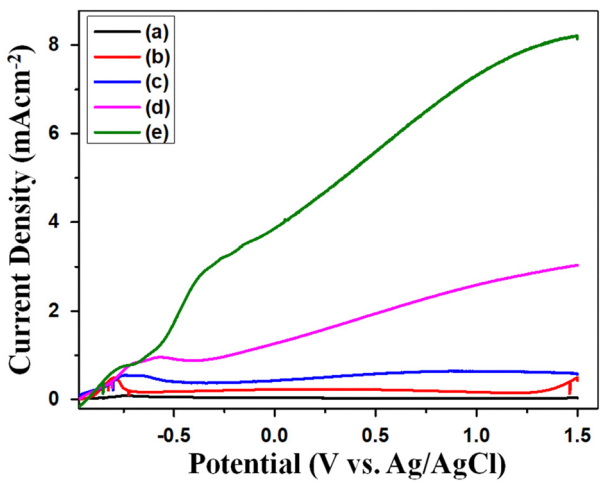

Fig. 5 *I–V* characteristics for (a) ZnO-dark, (b) ZnO-Illumination, (c) Zn(NP)-light, (d) Zn(NP)/ZnO(S)-illumination and (e) Zn(NP)/ZnO(R)-Illumination at an applied potential range of −1 V to 1.5 V performed in a 0.1 M Na_2SO_4 solution under solar AM 1.5 (100 mW cm^{-2}).

Table 2 Photocurrent densities at zero bias for different electrodes

S. no.	Photocatalyst	Current density (mA cm^{-2}) Dark	Illumination
1	ZnO	0.051	0.240
2	Zn(NP)	0.164	0.432
3	Zn(NP)/ZnO-S	0.450	1.26
4	Zn(NP)/ZnO-R	1.81	3.85

in Fig. 6(a). However, the probable reaction mechanism is depicted in Fig. 6(b) similar to that reported by Wang *et al.*[23] A series of steps that were involved are explained as follows:

$$Zn^{2+} + 4OH^- \rightarrow Zn(OH)_4^{2-} \quad (1)$$

$$Zn(OH)_4^{2-} \rightarrow ZnO_2^{2-} + 2H_2O(l) \quad (2)$$

$$Zn + 2OH^- \rightarrow ZnO_2^{2-} + H_2(g) \quad (3)$$

1. In the aqueous medium, Zn(NP) takes up the hydroxide ions which ultimately form ZnO_2^{2-} which later on act as the growth nuclei.

2. The ethanol helps ZnO_2^{2-} to be adsorbed onto the outer surface of the Zn(NP) due to favourable orientation of the Zn lattice.

3. Oxidation of Zn(NP) results in the formation of a layer of ZnO_2^{2-}.

4. The Kirkendall effect results in more and more diffusion of Zn(NP) to interact with hydroxide ions to form ZnO_2^{2-} with the simultaneous generation of hydrogen.

5. The extent of illumination and Zn/ZnO ratio leads to the formation of two different Zn/ZnO heterostructures recovered at different stages.

6. The working principle of the Zn(NP)/ZnO heterojunction is depicted with the energy band model (Fig. 6(b)). The band edges of Zn(NP) and ZnO were estimated by using the Butler–Ginley method.[24] Furthermore, illumination of (Zn/ZnO)-R leads to the generation of electrons and holes.

7. The holes may react with water to give protons and generate O_2 at the VB of ZnO while protons may be reduced by photoexcited electrons and generate hydrogen.

8. The distinguished photoelectrochemical performance can be explained on the basis of generated photocurrent along with the structural edge provided by the Zn/ZnO heterojunction.

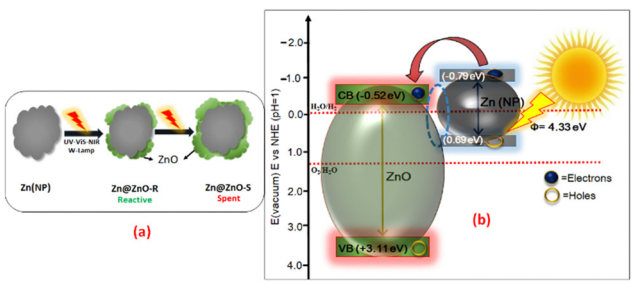

Fig. 6 (a) Schematic representation depicting the formation of the Zn/ZnO heterojunction. (b) Plausible mechanism depicting the effective charge separation.

Experimental section

Materials and methods

Zinc metal nanoparticles (Zn(NP)) of particle size 30–60 nm were procured from Nanoshel LLC, USA. 98% pure zinc oxide (ZnO) was purchased from Merck India. Double distilled water was used for all the experiments.

Synthesis of photoinduced Zn/ZnO nanoscale heterostructures

Photoinduced Zn/ZnO nanoscale heterostructures have been prepared *via* a simple route of illumination, wherein an appropriate light source (tungsten filament lamp) was used, which has the desired spectral characteristics (UV-Vis-NIR) matching the plasmonic peaks of Zn (UV and IR region).[14] A known amount of Zn(NP) was taken in a tubular borosilicate reactor, and nearly 100 mL of double distilled water was added to it. Cold water was circulated through the condenser fitted at the top of the photoreactor. Two tungsten filament lamps (200 W each) were used to illuminate the photoreactor externally. Nitrogen (N_2) gas was purged through a side port of the photoreactor to ensure an inert atmosphere throughout the synthesis. The concomitant hydrogen generated during the synthesis of Zn/ZnO heterostructures was monitored continuously through online gas chromatography (Carrier gas-N_2; Column-5A Molecular sieve; Detector-TCD).

At the beginning of the reaction, zinc (Zn) is in the form of Zn(NP). Upon illumination in the presence of water, a layer of ZnO is formed over Zn(NP). Optimization of the ZnO amount with respect to Zn(NP) is crucial, however, an optimum amount of Zn:ZnO leads to a higher reactivity in terms of the evolved H_2. The Zn(NP)/ZnO in its highly reactive (R) phase, where the HER was maximum, was named Zn(NP)/ZnO-R, while the Zn(NP)/ZnO heterostructures at which the HER was minimum revealing the low optimal ratio of Zn : ZnO indicative of the expending or spent (S) stage of Zn(NP) was represented as Zn(NP)/ZnO-S. The difference in the two structures was in terms of the amount of ZnO as well as the time of exposure to the incident radiation.

Characterization

A Rigaku Miniflex II Desktop model of X-ray diffractometer with Cu Kα radiation (l = 0.5405) was used to measure the X-ray diffraction (XRD) phases of Zn/ZnO based materials. The surface morphology of the Zn(NP)/ZnO-R and Zn(NP)/ZnO-S catalysts was examined by high-resolution transmission electron microscopy (HRTEM) (Model-JEM-2100F, JEOL, Japan). X-Ray photoelectron spectroscopy measurements were performed on a VSW spectrometer at a pressure of $<1 \times 10^{-9}$ torr with an Al Kα X-ray source (photon energy 1486.6 eV) at a pass energy of 20 eV.

Photoelectrochemical measurements

Photoelectrochemical (PEC) measurements of Zn(NP), ZnO, Zn(NP)/ZnO(R), and Zn(NP)/ZnO(S) samples were carried out by using a standard three-electrode configuration on a Zahner Zennium photoelectrochemical workstation (Zahner-Elektrik, Germany). These materials were screen printed on an indium tin oxide (ITO) glass substrate as per the protocol reported elsewhere.[25] These coated substrates were used as working electrodes. The platinum electrode was used as the counter electrode, and standard Ag/AgCl (3 N) acted as the reference electrode in the three-electrode system. However, 0.1 M sodium sulfate (Na_2SO_4) in an aqueous solution serves as an electrolyte. Solar light of AM-1.5G standard illumination was obtained from the solar simulator equipped with a 150 W xenon arc lamp.

Conclusions

In conclusion, photoinduced Zn/ZnO heterostructures were formed by illuminating zinc nanoparticles Zn(NP). The reactive Zn/ZnO heterostructure (Zn(NP)/ZnO-R) showed promising photoelectrochemical performance at zero bias, which may be attributed to several factors, including enhanced charge transfer, the formation of oxygen vacancies, and the SPR effect of zinc nanoparticles. The efficiency of the Zn/ZnO heterostructure as a photoanode material and concomitant generation of hydrogen resulting during their synthesis makes them attractive candidates for possible use in photocatalytic applications including solar energy conversion and efficient PEC performance. Thus, the Zn(NP)/ZnO-R acts as an efficient photoanode as evidenced by the increasing photocurrent density and most importantly, owing to the significant photocurrent density exhibited by the Zn/ZnO interface at zero bias, which is expected to be a more effective candidate for solar hydrogen generation.

Author contributions

Priti Mangrulkar: data curation, investigation, writing original draft, writing – review, and editing, visualization. Nilesh R. Manwar: investigation, visualization. Anushree Chilkalwar: investigation. Aparna Deshpande: resources. Sadhana Rayalu: conceptualization, supervision, project administration.

Conflicts of interest

The authors have no conflicts to declare.

Acknowledgements

This study was carried out within the framework of the CSIR Network Project (NWP-56). The authors acknowledge CSIR for financial support. NRM is thankful for PASIFIC postdoctoral funding received from the European Union's Horizon 2020 research and innovation program under the Marie Sklodowska-Curie grant agreement no. 847639 and from the Ministry of Education and Science.

Notes and references

1 R. S. Devan, R. A. Patil, J. H. Lin and Y. R. Ma, *Adv. Funct. Mater.*, 2012, **22**, 3326–3370.
2 S. Balanand, K. B. Babitha, M. J. Maria, A. Azeez, P. Mohamed and S. Ananthakumar, *ACS Sustainable Chem. Eng.*, 2018, **6**, 143–154.
3 D. Barreca, A. Gasparotto and E. Tondello, *J. Mater. Chem.*, 2011, **21**, 1648–1654.
4 A. Janotti and C. G. Van De Walle, *Rep. Prog. Phys.*, 2009, **72**, 126501.
5 Q. Xiang, F. Li, J. Wang, W. Chen, Q. Miao, Q. Zhang, P. Tao, C. Song, W. Shang, H. Zhu, T. Deng and J. Wu, *ACS Appl. Mater. Interfaces*, 2021, **13**, 10837–10844.
6 Y. Zhou, Z. Zhang, Z. Fang, M. Qiu, L. Ling, J. Long, L. Chen and Y. Tong, *Proc. Natl. Acad. Sci. U. S. A.*, 2019, **116**, 10232–10237.
7 H. Zeng, Z. Li, W. Cai, B. Cao, P. Liu and S. Yang, *J. Phys. Chem. B*, 2007, **111**, 14311–14317.
8 O. Lupan, L. Chow, G. Chai and H. Heinrich, *Chem. Phys. Lett.*, 2008, **465**, 249–253.
9 X. Y. Kong, Y. Ding and Z. L. Wang, *J. Phys. Chem. B*, 2004, **108**, 570–574.
10 S. Hsu, Y. Chen, C. Ye, I. Tseng and L. Chao, *Sens. Actuators, B*, 2014, **204**, 175–182.
11 W. S. Khan, C. Cao, Z. Chen and G. Nabi, *Mater. Chem. Phys.*, 2010, **124**, 493–498.
12 D. Tang, G. Liu, F. Li, J. Tan, C. Liu, G. Q. Lu and H. Cheng, *J. Phys. Chem. C*, 2009, **113**, 11035–11040.
13 W. Tang, D. Huang, L. Wu, C. Zhao, L. Xu, H. Gao, X. Zhang and W. Wang, *CrystEngComm*, 2011, **13**, 2336–2339.
14 A. Sajjad, S. H. Bhatti, Z. Ali, G. H. Jaffari, N. A. Khan, Z. F. Rizvi and M. Zia, *ACS Omega*, 2021, **6**, 11783–11793.
15 M. Santos Anholeti, A. Rocha Honorio de Oliveira, J. Castro da Cruz, V. Andrade Luciano, M. Aparecida Nascimento, G. Alves Puiatti, A. P. de Carvalho Teixeira and R. Pereira Lopes, *Mater. Chem. Phys.*, 2022, **284**, 126058.
16 R. R. Bhosale, *Int. J. Hydrogen Energy*, 2021, **46**, 4739–4748.
17 H. Amekura, N. Umeda, K. Kono, Y. Takeda and N. Kishimoto, *Nanotechnology*, 2007, **18**, 395707.
18 H. Amekura, M. Tanaka, Y. Katsuya, H. Yoshikawa, H. Shinotsuka, H. Amekura, M. Tanaka, Y. Katsuya, H. Yoshikawa, H. Shinotsuka and S. Tanuma, *Appl. Phys. Lett.*, 2010, **96**, 023110.
19 A. Bera, T. Ghosh and D. Basak, *ACS Appl. Mater. Interfaces*, 2010, **2**, 2898–2903.
20 B. Paul, S. Vadivel, N. Yadav and S. S. Dhar, *Catal. Commun.*, 2019, **124**, 71–75.
21 Z. Yin, X. Wang, F. Sun, X. Tong, C. Zhu, Q. Lv, D. Ye, S. Wang, W. Luo and Y. A. Huang, *Sci. Rep.*, 2017, **7**, 1–10.
22 M. Adeel, M. Saeed, I. Khan, M. Muneer and N. Akram, *ACS Omega*, 2021, **6**, 1426–1435.
23 Z. Wang, F. Wang, Y. Lu, M. Xu and Q. Li, *J. Exp. Nanosci.*, 2016, **11**, 383–394.
24 M. A. Butler, D. S. Ginley, J. E. Soc, M. A. Butler and D. S. Ginley, *J. Electrochem. Soc.*, 1978, **125**, 228–232.
25 F. Qiao, L. Lu, P. Han, D. Ge, Y. Rui, D. Gu, T. Zhang, J. Hou and Y. Yang, *Sci. Rep.*, 2020, **10**, 1–11.